Brazilian Dental Science

unesp
UNIVERSIDADE ESTADUAL PAULISTA
"JÚLIO DE MESQUITA FILHO"
Instituto de Ciência e Tecnologia
Campus de São José dos Campos

Original Article

DOI: https://doi.org/10.4322/bds.2026.e5047

3D-printed inorganic-filled resin under hydrothermal aging with different post-polymerization times: microstructure, optical, and mechanical properties

Resina de impressão 3D com carga inorgânica sob envelhecimento hidrotérmico com diferentes tempos de pós-polimerização: microestrutura, propriedades ópticas e mecânicas

Laura Viviana Calvache ARCILA[1], Tiago Moreira Bastos CAMPOS[2], Joyce Roma Corrêia dos Santos SIQUEIRA[1], Marco Antonio BOTTINO[1], Nathália de Carvalho RAMOS[1]

1 - Universidade Estadual Paulista, Instituto de Ciência e Tecnologia, Departamento de Materiais Odontológicos e Prótese. São José dos Campos, SP, Brazil.
2 - Instituto Tecnológico de Aeronáutica, Departamento de Física. São José dos Campos, SP, Brazil.

How to cite: Arcila LVC, Campos TMB, Siqueira JRCS, Bottino MA, Ramos NC. 3D-printed inorganic-filled resin under hydrothermal aging with different post-polymerization times: microstructure, optical, and mechanical properties. Braz. Dent. Sci. 2026;29:e5047. https://doi.org/10.4322/bds.2026.e5047

ABSTRACT

Objective: This study aims to characterize and evaluate the optical and mechanical properties of a 3D-printed resin (NanoLab, Wilcos) at different post-polymerization times (0, 16, 32, and 60 minutes) before and after hydrothermal aging. **Material and Methods:** Characterization was performed via Scanning Electron Microscopy (SEM), energy spectroscopy (EDX), gravimetry to determine the chemical composition and inorganic filler content, and Fourier-transform Infrared Spectroscopy (FT-IR) to identify the degree of conversion of the resin (n=6). For mechanical and optical properties, flexural strength (n=8), microhardness (n=3), elastic modulus (n=3), color, and translucency (n=6) (CieLab2000) were measured. **Results:** Results showed that the microstructure reveals surface porosities. The organic matrix and inorganic filler contents of the resin were 46.75%, and 53.24%, respectively. Increasing post-polymerization time improved the degree of conversion and resulted in significant differences in mechanical properties and color stability ($p < 0.001$), whereas hydrothermal aging reduced hardness and elastic modulus but increased flexural strength. **Conclusion:** It was concluded that both the mechanical and optical behavior of the printed resin are significantly influenced by microstructure, chemical composition, post-polymerization times, and hydrothermal aging. A suggested suitable post-polymerization time is 32 minutes to ensure clinically acceptable color stability and achieve good mechanical properties, although this may impact the translucency of the material. The 3D- printed resin exhibited suitable properties for long-term dental restorations.

KEYWORDS

3D printing; Aging; Dental material; Dental resin; Flexural strength; Mechanical tests; Polymerization.

RESUMO

Objetivo: Este estudo tem como objetivo caracterizar e avaliar as propriedades ópticas e mecânicas de uma resina para impressão 3D (NanoLab, Wilcos) em diferentes tempos de pós-polimerização (0, 16, 32 e 60 minutos) antes e depois do envelhecimento hidrotérmico. **Material e Métodos:** A caracterização foi realizada por meio de Microscopia Eletrônica de Varredura (MEV), espectroscopia de energia (EDX), gravimetria para determinar a composição química e o teor de carga inorgânica da resina, e Espectroscopia de Infravermelho com Transformada de Fourier (FT-IR) para identificar o grau de conversão da resina (n=6). Para propriedades mecânicas e ópticas, foram medidas a resistência à flexão (n=8), a microdureza (n=3), o módulo de elasticidade (n=3), a cor e a translucidez (CieLab2000) (n=6). **Resultados:** Os resultados mostraram que a microestrutura

revela porosidades superficiais. O conteúdo de matriz orgânica e da carga inorgânica da resina foi de 46,75% e 53,24%, respectivamente. O aumento do tempo de pós-polimerização melhorou o grau de conversão e resultou em diferenças significativas nas propriedades mecânicas e na estabilidade de cor ($p < 0,001$), enquanto o envelhecimento hidrotérmico reduziu a dureza e o módulo elástico, mas aumentou a resistência à flexão. **Conclusão:** Concluiu-se que tanto o comportamento mecânico quanto o óptico da resina de impressão 3D são significativamente influenciados pela microestrutura, composição química, tempos de pós-polimerização e envelhecimento hidrotérmico. Um tempo de pós-polimerização adequado sugerido é de 32 minutos para garantir uma estabilidade de cor clinicamente aceitável e obter boas propriedades mecânicas, embora isso possa afetar a translucidez do material. A resina para impressão 3D apresentou propriedades adequadas para restaurações dentárias de longa duração.

PALAVRAS-CHAVE

Impressão 3D; Evelhecimento; Materiais dentais; Resina dental; Resistência à flexão; Testes mecânicos; Polimerização.

INTRODUCTION

Technological advancements driven by computational engineering, such as CAD/CAM (Computer-aided design/computer-aided manufacturing), have had a transformative impact on dentistry. The additive technique through 3D printing, also known as rapid prototyping, creates parts by adding sequential layers, eliminating geometric limitations that could hinder printing. Additionally, it allows for the creation of intricate details and complex internal geometries that would be restricted by subtractive manufacturing methods [1-6].

3D printing has already become popular in dentistry for the fabrication of dental models, surgical guides, occlusal devices, and also for the full crowns production, partial restorations, veneers, and fixed prostheses [3,4,7,8]. To achieve long-term dental restorations, ceramic nanoparticles have been incorporated into the resins used in 3D printing. These resins are primarily composed of acrylic-based photopolymers [9-12]. The introduction of inorganic fillers, such as ceramic nanoparticles, can enhance both the mechanical and aesthetic properties of the 3D-printed resins. This includes increasing flexural strength, elastic modulus, and Vickers hardness. Additionally, post-polymerization times can cause variations in the material's color [13-15].

On the other hand, the influence of hydrothermal aging on polymeric resins for temporary restorations has been widely investigated in the literature. This process can significantly impact the physical properties of resins, based on their composition, processing parameters, manufacturing method, and aging protocol [16-19], with an observed increase in flexural strength after this process [20]. However, few studies have investigated these properties under thermocycling conditions for final (long-term) restorations using 3D-printed resins.

The post-polymerization process is another factor extensively studied in the literature on 3D-printed resins, as it is directly related to their mechanical behavior and optical properties. Studies report variability in the recommended post-polymerization time to achieve acceptable clinical performance. However, a duality between these two properties may exist, while longer post-polymerization times tend to improve mechanical properties, they can negatively impact color stability, reaching a clinically unacceptable level [13,21].

It is crucial to highlight that understanding the chemical composition and characterizing the printing material is necessary to encompass not only its mechanical behavior but also its optical properties. These properties play a fundamental role in achieving satisfactory performance for long-term restorations used in the oral cavity.

The objective of this study was to characterize the microstructure, the optical and mechanical properties of a 3D-printed resin for long-term restorations at different post-polymerization times (0, 16, 32, and 60 minutes) before and after hydrothermal aging. The null hypothesis of this study is that the post-polymerization time and hydrothermal aging do not significantly affect the mechanical properties, optical properties and microstructural characteristics of the 3D-printed resin.

MATERIALS AND METHODS

Specimen preparation

The sample numbers were based on studies found in the literature for elastic modulus [22], microhardness [23], color and translucency [24], and degree of conversion by FT-IR tests [25]; for the flexural test, the sample calculation was performed considering 5% alpha error, 80% minimum acceptable power, and considering the analysis for 8 independent groups (G*Power 3.1.9.3 for Mac OS Tahoe, Düsseldorf, Germany). Bars measuring 25 x 10 x 2 mm (n=8) for flexural testing, following the International Standard Organization (ISO 4049–2019), 60 x 10 x 5 mm (n=3) according to the Bertassoni et al. methodology [26], for elastic modulus and microhardness, and squares measuring 2 x 2 x 2 mm (n=6), following the methodology adapted from Ramos et al. [27], for color, translucency, and FT-IR (Fourier Transform Infrared Spectroscopy) measurements were designed using modeling software (Rhinoceros 6.0 SR8 McNell North America, USA). The designs were saved in STL (Standard Tessellation Language) files and exported to the specific software for the 3D printer to be printed with the inorganic-filled resin (Manufacturer's information: Nanolab Resin, Wilcos, Brazil- Batch Nº: 2209036; nanohybrid resin; shade A1). The samples were sliced using the Photon Workshop 64 V2.129. RC 12 software for the LCD printer (Anycubic Photon Mono Se 3D) with printing parameters shown in Table I, and the experimental design in the Figure 1.

The supports of the samples were manually removed and then subjected to the post-processing phase. During this step, the samples were washed in isopropyl alcohol for 4 minutes to remove residual monomers from the surface. After cleaning, the samples were divided into four post-polymerization time groups: 0 minutes, 16 minutes, 32 minutes, and 60 minutes, in a cure rotary washer machine (Wash & Cure 2.0, Anycubic 3D – 25,000 mW, LED, 30.5 mm2, 405 nm, 819.6 mW/mm2), according to the manufacturer. The samples were then polished with SiC paper (#800, 1200, and 2000) on a polishing machine (Buelher Ecomet 250) [20].

Table I - Printing parameters used in the study

Configuration	Parameter
Layer thickness	0.050 mm
Normal exposure time	1.50 s
off time	0.50 s
Lower exposure time	30.00 s
Lower layers	6
Lifting Distance Z	6 mm
Lifting speed Z	4 mm/s
Retraction speed Z	6 mm/s
Slice Shape	
Contact depth	0.05 mm
Contact diameter	1.50 mm
Shape	Pyramid
Diameter	2.20 mm
Length	4 mm
Angle	90°
Support Parameters	
Support	Medium
Automatic support angle	30°
Density	69%
Minimum length	5 mm

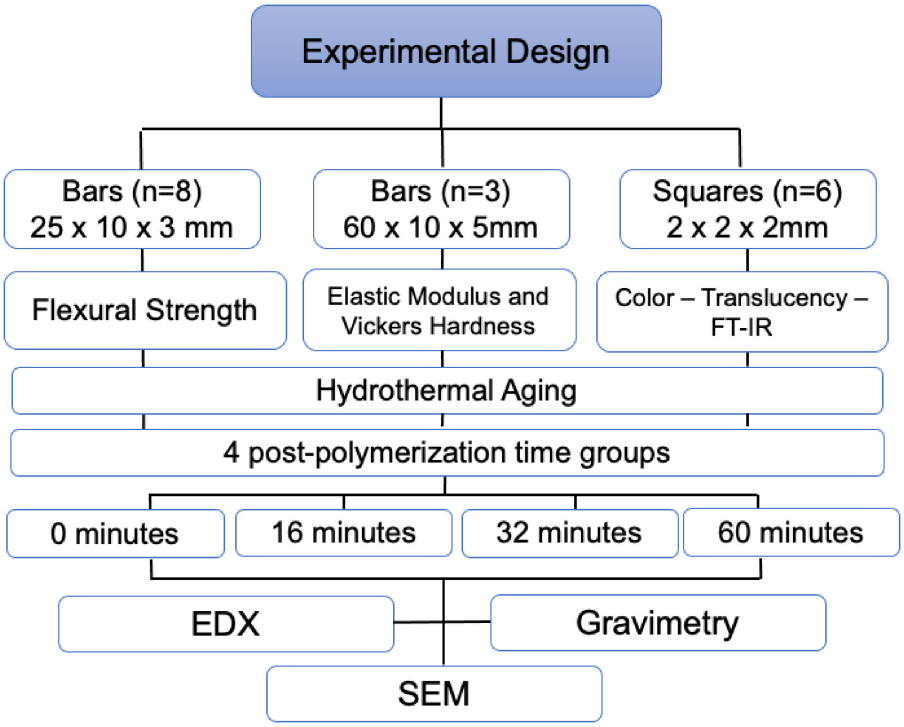

Figure 1 - Study design.

Scanning electron microscopy and energy-dispersive X-ray spectroscopy

Representative specimens from each post-polymerization group (n=3) were analyzed for their surface characteristics using a scanning electron microscope (SEM Inspect S50, FEI Company, Brno, Czech Republic) at 4000x magnification and current of 25.0 KV. Chemical analysis was also performed by energy-dispersive X-ray spectroscopy (EDX) coupled with the SEM to identify the surface chemical microconstituents at a magnification of 20.0 kx and current of 20.0 KV.

Gravimetry

Gravimetric analysis was used to quantify the inorganic particle volume in the 3D-printed resin, following a protocol adapted from Adabo et al. [28]. Initially, a square sample (0.77 g) was weighed using a precision balance (OHAUS, Adventurer). Subsequently, a refractory was weighed on the same balance (1.315 g). The sample along with the refractory was placed in a wax elimination furnace (F-3000 5P, EDG, 220V) at a maximum temperature of 600°C for 1 hour and 30 minutes. Afterward, the sample with the refractory was reweighed on the balance (1.356 g), and the weight of the refractory was subtracted to determine the final weight of the calcined sample, which was 0.41 g.

Fourier transform infrared spectroscopy (FT-IR)

Squares measuring 2 x 2 x 2 mm (n=6) were analyzed by FT-IR to assess the degree of conversion of the different post-polymerization groups before and after hydrothermal aging. The pieces were positioned in the ATR (Specac Ltd., UK) rings placed on a diamond crystal plate, and the final IR spectra were collected using the FT-IR and processed with Origin Pro 8.5 software.

Each spectrum was obtained in absorbance mode by accumulating 32 scans covering wavelength bands between 1700 and 1600 cm^{-1}, corresponding to carbonyl and aliphatic double bonds [29]. The degree of conversion was determined based on the carbon double bonds present in the spectra (% C=C) of the different post-polymerization time groups, both before and after hydrothermal aging.

To determine the polymeric composition of the resin, the spectrum of the resin in the liquid phase was analyzed, using wavelength bands between 1200-1700 cm^{-1}. The chemical structures of the monomers were compared and confirmed with those studied in the work by

Delgado et al. [30]. According to their methodology, FT-IR spectra of individual monomers such as 10-methacryloyloxydecyl dihydrogen phosphate (10-MDP, DMHealthcare, San Diego, CA, USA, code P01030), 2-hydroxyethyl methacrylate (HEMA, DMG, Hamburg, Germany, code 11220), Bis-GMA (Polysciences, Warrington, PA, USA, code 03344), UDMA (DMG, Hamburg, Germany, code 100112), and TEGDMA (DMG, Hamburg, Germany, code 100102) were obtained. For each monomer, the chemical structure was elaborated, enabling the identification of methacrylate peaks and the interpretation of results (Table II).

Flexural strength

Flexural strength was determined using a three-point bending test according to the International Standard Organization (ISO 4049,2019). A universal testing machine (Emic DL-1000, Emic, Brazil) with a 100 Kgf load cell and a speed of 0.5 mm/s was used, and load was applied until bar fracture (n=8). The flexural strength (MPa) was calculated according to the following equation:

$$\sigma = (3FI) / \left(2bh^2\right) \quad (1)$$

Where F is the load in N, l is the span between supports (20 mm), b is the width (10 mm) of the specimen, and h is the thickness (2 mm) of the specimen at the fracture origin in mm [31,32].

Elastic modulus and vickers hardness

First, the dry mass of the samples (n=3) was measured using a precision balance, and then the test was applied using a Sonelastic® equipment (ATCP Engenharia Física, Brazil) by the impulse excitation technique. On the same samples, three indentations were made on the upper and lower surfaces using a Vickers diamond indenter with a 300g load for 15 seconds. The diagonals of the indentation marks were then measured using a microscope attached to the hardness tester (20x).

Color change and translucency parameters

A spectrophotometer (EasyShade Advance 4.0) was used to measure color and translucency (n=6) through the L (lightness), a (redness), and b (greenness) parameters (CIE, Commision Internationale de l'Eclairage) with black (L* = 18, a* = 13, b* = −15) and white (L* = 95.7, a* = −13, b* = 2.6) backdrops for translucency and gray backdrop for color. To ensure optical continuity, a drop of glycerol was placed between the specimen and the backdrop. The translucency parameter (Tp) was calculated according to the following formula:

$$Tp = \left[\begin{array}{l} \left(L\_b^* - L\_p^*\right)^2 + \left(a\_b^* - a\_p^*\right)^2 \\ + \left(b\_b^* - b\_p^*\right)^2 \end{array} \right] \quad (2)$$

Subscript "p" refers to color coordinates on the black background, and subscript "b" refers to those on the white background. The color coordinates of the backgrounds were: white (L:84.95; a:-0.38; b:2.93) and black (L:25.58; a:-0.15; b:-0.24). The color difference was calculated using the CIEDE2000 formula (ΔE00) [33]:

$$\Delta E' = \left[\left(\frac{\Delta L'}{K_L S_L}\right)^2 + \left(\frac{\Delta C'}{K_C S_C}\right)^2 + \left(\frac{\Delta H'}{K_H S_H}\right)^2 + R_T \left(\frac{\Delta C'}{K_C S_C}\right)\left(\frac{\Delta H'}{K_H S_H}\right) \right]^{1/2} \quad (3)$$

Where ΔE represents the differences in lightness, chroma, and hue for the samples (before and after aging) in CIEDE2000, and RT is a function responsible for the interaction between chroma and hue differences in the blue region. Weighting functions SL, SC, and SH adjust the total color

Table II - FT-IR Attribution

Wavelength (cm^{-1})	Attribution	Chemical Component
1700 - 1600	C=O	Carbonyl
1638 - 1632	C=C	Alkene
1720 - 1700	C=O	Ester
1450 - 1375	CH_2 and CH_3	Methylene and Methyl
1250 - 1200	C-O-C	Ether
1160 - 1120	P=O	Phosphate
1070 - 1010	Si-O	Siloxane

difference for variations in the color difference pair's location in the L, a, and b coordinates, and the parametric factors KL, KC, and KH are correction terms for experimental conditions [27,34].

Hydrothermal aging

The printed specimens of each post-polymerization group (Immediate Group), after all previous tests, were aged (Aged Group) by 5,000 thermocycles in water, with bath times of 30 seconds at 5 °C and 55 °C, with a transfer time of 5 seconds in a thermal cycler (Termocycle Biopdi, Brazil) [20], to determine the susceptibility to degradation by hydrothermal aging.

Statistical analysis

Normality tests (Kolmogorov-Smirnov, Shapiro-Wilk) and Levene's test (95%) showed that the data were normal and homoscedastic ($p > 0.05$) for hardness, elastic modulus, flexural strength, color, and translucency data. Two-way ANOVA and Tukey post-hoc tests (Minitab 19, Minitab Inc., USA) were applied for the same data, except for the color change test, which used One-way ANOVA. A significance level of 5% was used for all analyses. Hydrothermal aging degradation and gravimetry (%) were calculated as the percentage of the immediate and aged groups to analyze the organic and inorganic load, respectively.

RESULTS

Figures 2 and 3 show the FEG-SEM micrographs. Figure 2 shows the microstructure of the 3D-printed resin, where the blue arrow points to the polymeric particles, constituting the organic phase, while the yellow and black arrows indicate the micrometric and nanometric

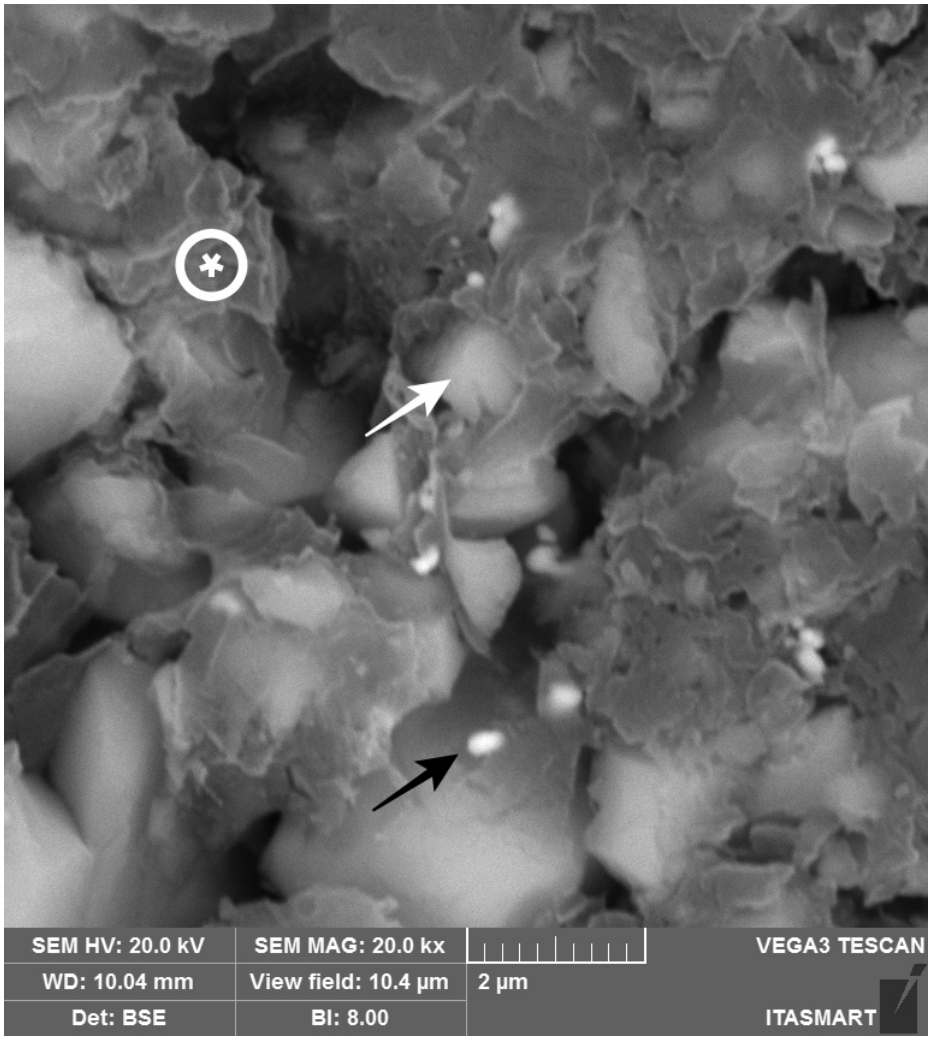

Figure 2 - The micrograph is at a magnification of 20kx and current of 20.0 kV. The asterisk indicates the polymeric particles region, which are the organic phase of the 3D- Printed resin; the white and black arrows point to the micrometric and nanometric glass particles, respectively, which are the inorganic phase of the resin.

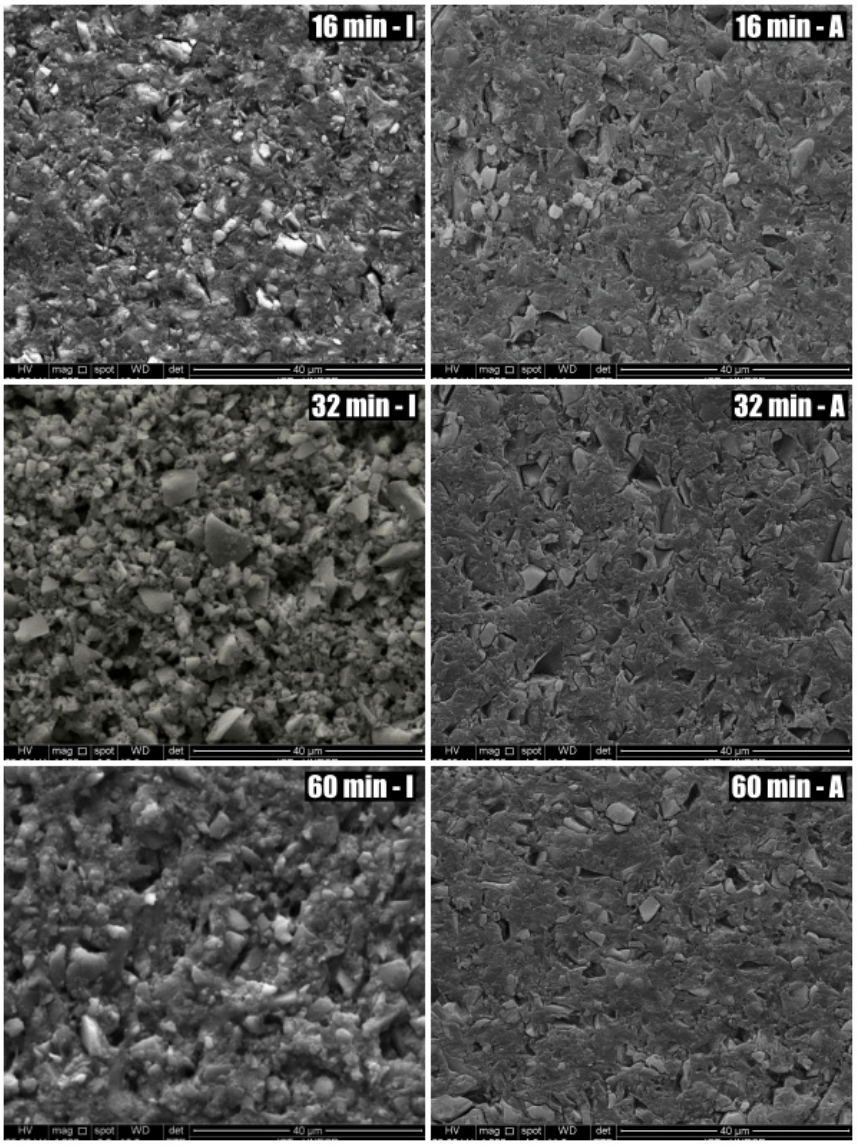

Figure 3 - The micrographs are shown at 4000x magnification and current of 25.0 kV. The left column shows the micrographs of the 3D-Printed resin in the initial post-polymerization groups (I), and the right column shows the material after hydrothermal aging (A).

glass particles respectively, corresponding to the inorganic filled. Figure 3 shows the microstructure of the 3D-printed resin from the Initial (I) and aged (A) post-polymerization groups. It can be seen that the superficial characteristics are similar. However, they present particles with acute angles, uniformly distributed, and porosities on their surface. The initial 32-minutes group exhibits more evident particles. Furthermore, no differences were recognized in their morphology before and after hydrothermal aging.

In Table III, it is possible to observe the degree of conversion of each initial and aged post-polymerization group, and the degradation after hydrothermal aging, which indicates that as the post-polymerization time increases, the degree of conversion also increases, being the lowest for the non-post-polymerization group (56.93%), and the highest for the 60-minute group (68.03%). Degradation comparison to the immediate groups was greater for group non-post- polymerization (26.96%), and lower for the 60 min group (18.77%).

The polymeric composition of the 3D-printed resin consists of triethylene glycol dimethacrylate (TEGDMA) and urethane dimethacrylate (UDMA), as evidenced by the FT-IR spectrum, presented in Figure 4. This spectrum reveals the same peaks associated with these two monomers, covering wavelengths in the range of 1200-1700 cm^{-1}.

Table IV shows the chemical composition (%) of the 3D-printed resin obtained by EDX, including the percentage of organic (46.75%) and inorganic (53.24%) filler, obtained by gravimetry.

Table III - Percentages of the degree of Conversion and degradation upon hydrothermal aging of the different initial and aged post-polymerization groups

Post-polymerization times	Conversion Degree (%)		Degradation (%)
	Initial	Aged	
0 min	56.93	83.90	26.96
16 min	60.70	86.08	25.38
32 min	66.58	86.50	19.92
60 min	68.03	86.80	18.77

Table IV - Percentages of the chemical composition of 3D- Printed resin

Chemical Comoposition	(%) 3D- Printed Resin	(%) Fired Resin	(%) Organic Filler	(%) Inorganic Filler
Carbon	44.0%	-	46.75%	53.24%
Oxygen	37.6%	-		
Silica	7.8%	60.9%		
Barium	9.2%	29.6%		
Aluminium	1.4%	9.6%		

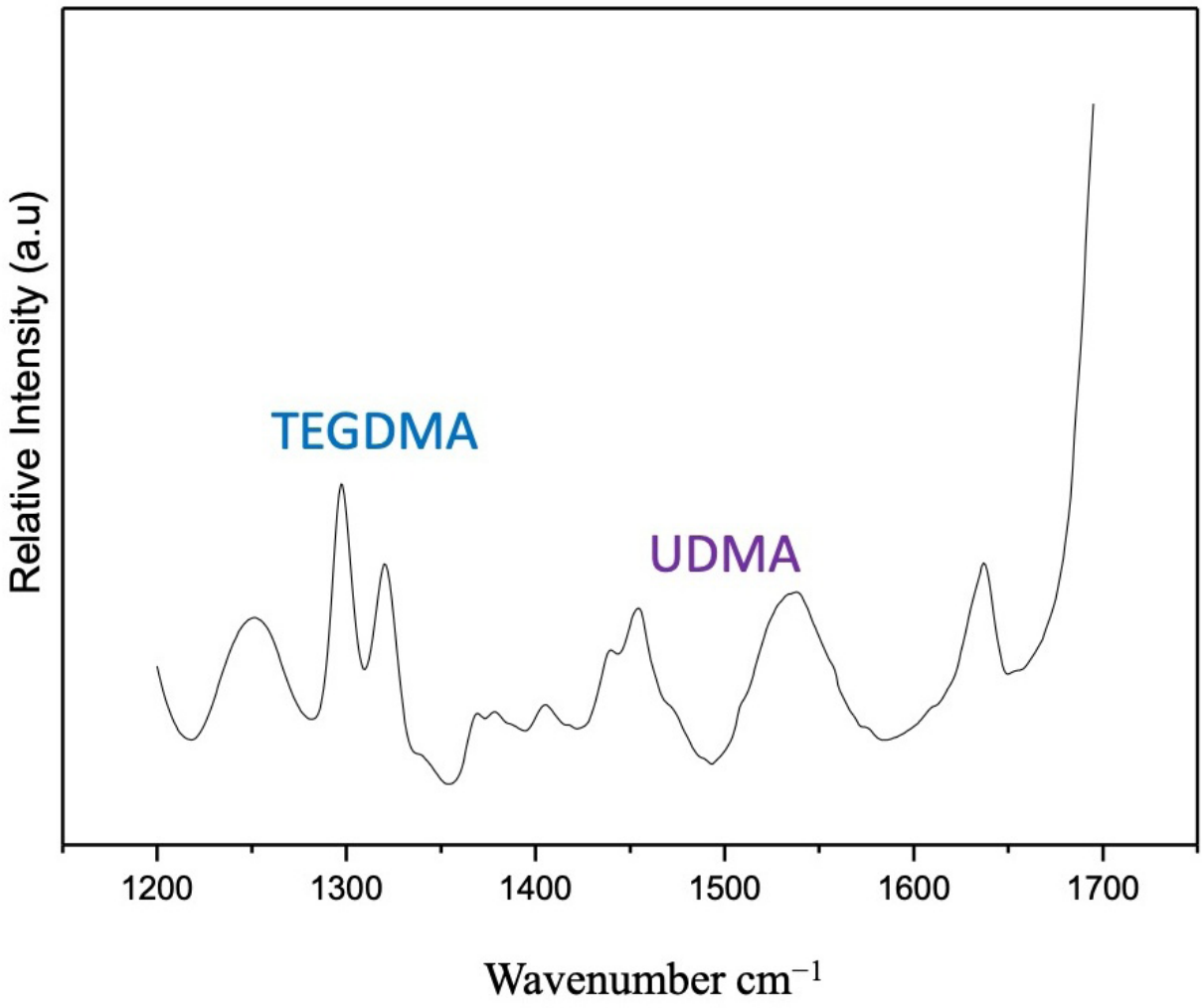

Figure 4 - FT-IR spectrum of the polymer composition of the 3D-Printed resin.

Table V - Mean and standard deviation of the 3D- Printed resin at different post-polymerization times in relation to flexural strength, hardness and elastic modulus (before and after hydrothermal aging)

Post-Polymerization Times	Flexural Strength (MPa)		Vickers Hardness (HV)		Elastic Modulus (GPa)	
	Initial	Aged	Initial	Aged	Initial	Aged
0 Min	102.35 ± 8.16^{C}	66.38 ± 5.47^{D}	26.12 ± 2.13^{B}	11.4 ± 0.75^{D}	9.39 ± 0.29^{A}	6.15 ± 0.44^{B}
16 Min	132.72 ± 8.89^{AB}	118.03 ± 7.55^{BC}	34.23 ± 1.28^{A}	14.89 ± 1.06^{C}	9.59 ± 0.13^{A}	6.09 ± 0.64^{B}
32 Min	134.00 ± 8.96^{AB}	129.15 ± 11.16^{AB}	34.13 ± 0.74^{A}	14.53 ± 0.76^{C}	9.47 ± 0.40^{A}	7.16 ± 1.0^{B}
60 Min	110.64 ± 13.15^{C}	137.33 ± 7.96^{A}	33.56 ± 3.36^{A}	16.31 ± 1.70^{C}	9.48 ± 0.13^{A}	7.17 ± 0.22^{B}

Different letters represent statistically significant differences, Two way ANOVA and Tukey test ($p<0.05$).

Table VI - Mean, standard deviation and confidence intervals of the color, mean and standard deviation of translucency of the 3D-Printed resin of different post-polymerization times, before and after hydrothermal aging

Post-Polymerization Time	Color (ΔE_{00})	95% CI	Translucency (Initial)	Translucency (Aged)
0 Min	13.06 ± 2.79^{A}	10.65–15.47	21.86 ± 6.16^{A}	5.93 ± 0.37^{BC}
16 Min	15.02 ± 9.53^{A}	12.79–17.25	8.63 ± 6.28^{B}	5.43 ± 0.67^{C}
32 Min	2.53 ± 0.50^{B}	0.44– 4.62	6.96 ± 0.64^{BC}	5.23 ± 0.63^{C}
60 Min	5.67 ± 2.14^{B}	3.26– 8.08	5.48 ± 1.75^{C}	4.64 ± 0.70^{C}

Different letters represent statistically significant differences, One way ANOVA for color, and two way ANOVA for Translucency, Tukey test ($p<0.05$).

On the other hand, the flexural strength of the resin had a statistically significant differences, were found for post-polymerization time ($p < 0.001$), for the interaction between factors ($p < 0.001$), and for hydrothermal aging ($p = 0.011$). The aged 0-minute group showed the lowest flexural strength, whereas the aged 60-minute group, although statistically similar to the initial 16- and 32-minute groups and the aged 32-minute group, exhibited the highest mean flexural strength (Table V).

The material hardness showed a statistically significant difference ($p < 0.001$) for both post-polymerization time and aging. The groups before aging (Initial) presented the highest hardness values, while the 0 minutes aged groups presented the lowest value (Table V). The elastic modulus showed a statistically significant difference ($p < 0.001$) only for groups before and after hydrothermal aging. The Initial groups had a greater elastic modulus, while the aged ones had a lower value, as illustrated in Table V.

As for optical properties, both color and translucency had a statistically significant difference $p < 0.001$. In terms of color, the 32- and 60-min groups had greater color stability. In terms of translucency, the 0-min initial group showed the highest translucency and the 60 min group had the lowest translucency, while all aged groups were similar (Table VI).

DISCUSSION

This study evaluated a 3D-printed inorganic-filled resin intended for long-term restorations, considering its microstructure, degree of conversion, optical and mechanical properties at different post-polymerization times after hydrothermal aging. The results showed significant differences and rejected the null hypothesis.

The results of this study indicate that post-polymerization time significantly influences the mechanical and optical properties of the 3D-printed inorganic-filled resin. Increasing the post-polymerization time led to a higher degree of conversion and improvements in mechanical properties, such as flexural strength and hardness. This is consistent with previous studies showing that longer post-polymerization times result in greater monomer conversion, reducing water sorption susceptibility and the amount of residual monomers, thereby improving the structural integrity of the material [16,17]. For polymer-based materials, a degree of conversion of approximately 50% is required to ensure the applicability and clinical success

of dental restorations [35]. Based on this, in the present study, the 3D-printed inorganic-filled resin achieved an ideal conversion rate for clinical use (Table III). The increase in the degree of conversion in the different post-polymerization groups after hydrothermal aging can be attributed to the rise in temperature, which in turn enhances molecular mobility within the system. This enables unreacted monomers, unpolymerized double bonds, and photoinitiators to continue the polymerization process [36-38].

Due to the hydrolytic degradation that polymeric materials undergo during hydrothermal variations in the oral cavity, their properties are altered, affecting their mechanical behavior over time. Additionally, their chemical composition and manufacturing method can also influence these properties [32]. Flexural strength showed a significant difference; in the group post-polymerization for 60 minutes and subjected to aging, despite being similar to the initial 16- and 32-minute groups and the 32-minute aged group, it presented the highest mean flexural strength (137.33 ± 7.96 MPa), while the aged group without post-polymerization showed the lowest strength (66.38 ± 5.47 MPa). This may be due to the water absorption process in the early stages of aging that the resin underwent, which exhibited ductile behavior and allowed plastic deformation before fracture. This could explain the high aging resistance of the resin. In later stages of water absorption, there is a progressive degradation of the polymer's mechanical properties due to the softening of the polymer matrix, as water molecules penetrate the spaces between polymer chains, acting as plasticizers and, by separating these chains, make the matrix softer [17,20,33].

On the other hand, the hydrothermal aging protocol used in this study was based on those described by Bergamo et al. [20] and Gale and Darvell [39], consisting of 5,000 thermal cycles in water with 30-second immersion times at 5 °C and 55 °C, simulating approximately six months of intraoral conditions. The findings of Bergamo et al. (2022), indicated that, although hydrothermal aging increased the flexural strength of different polymer systems (conventional, milled, and printed), no significant differences were observed among the printed resins evaluated [20]. In contrast, Keßler et al. [19] employed two aging protocols: storage in distilled water at 37 °C for 24 hours, followed by thermocycling between 5 °C (±2) and 55 °C (±2) for 10,000 cycles, with a dwell time of 30 seconds and a transfer time of 5 seconds. Their results demonstrated that three printed resins, with and without filler and from different commercial brands, exhibited reduced strength after hydrothermal aging. These discrepancies among studies may be attributed to the lack of standardization in hydrothermal aging protocols and methodologies. Nevertheless, it is evident that hydrothermal aging has a direct impact on the physical and mechanical properties of 3D-printed resins [19,20].

The data also showed that hydrothermal aging negatively impacts the hardness and elastic modulus of the 3D- printed resin, which can be attributed to water absorption and subsequent plasticization of the polymer matrix [32,40]. However, an increase in flexural strength was observed after aging, especially in the post-polymerization 60 minutes group. This may be explained by the initial water absorption, which can cause plastic deformation before fracture, increasing the material's toughness, affecting surface properties, and promoting plasticization—resulting in a less rigid and consequently more plastic resin [41]. Other studies in the literature support this finding, showing that hardness and elastic modulus values after aging can reach as low as half of their initial values [32,40].

It has been demonstrated that modifying the chemical composition of 3D-printed resins by adding nanoparticles filled with glass to the polymer matrix significantly improves their physical and mechanical properties [10-12]. Through the analysis performed using EDX, along with gravimetric analysis of the 3D-printed resin in this study, it was observed that the resin has an inorganic filler content of 53.24%, composed mainly of silica, barium, and aluminum, with silica being the most abundant element, reaching 60.9%. This finding is supported by the SEM micrograph (Figure 2), in which micro- and nano-sized glass particles are visible in the material's microstructure. In the study by Borella et al. [9], 3D-printed resins indicated for temporary and long-term restorations were compared to confirm that the presence of inorganic filler in the chemical composition contributes to improved mechanical properties. This is evident when observing that the resin recommended for temporary restorations was unfilled, resulting in inferior physical and mechanical properties compared to resins containing inorganic

micro fillers [9]. It is important to clarify that, although the manufacturer recommends the 3D-printed resin investigated in this study for long-term restorations, other factors such as fatigue resistance, wear behavior, and bonding performance should also be considered.

In turn, the SEM micrographs in Figure 3 show the surface characteristics of the 3D-printed resin at different post-polymerization times. Although no visible differences were observed on the surface after hydrothermal aging, the resin exhibits irregularly shaped angular grains distributed throughout its morphology, along with surface porosities and non-homogeneous areas. Some studies have shown that the presence of such features in filled polymeric materials can increase the likelihood of crack formation due to the non-uniform distribution of mechanical stresses. As a result, these characteristics can influence the physical and mechanical behavior, making layer-printed materials more prone to delamination [9,15,42].

On the other hand, the polymeric composition of the studied resin includes UDMA and TEGDMA monomers, as evidenced by the FT-IR spectrum in Figure 4. Regarding this composition and the water sorption phenomenon that occurs during hydrothermal aging, it is likely that the mechanical properties are affected [20]. In this study, the post-polymerization groups aged for 60 and 32 minutes showed less degradation during hydrothermal aging (18.77% and 19.92%, respectively), releasing fewer residual monomers such as UDMA. Furthermore, after undergoing water sorption, these groups showed reduced surface defects, generating compressive stress on the surface, which resulted in increased flexural strength [20]. In contrast, the 0-minute aged group experienced the highest degradation (26.96%). Although it also absorbed water, it released more residual monomers, which led to lower flexural strength, hardness, and elastic modulus [20] (Table IV). Therefore, it can be inferred that both hydrothermal aging and the chemical composition of the resin influence its mechanical properties [17-20].

Color stability is a crucial factor for the clinical acceptability of dental restorations. The post-polymerization groups of 32 and 60 minutes showed color stability within the acceptable limits established by ISO/TR 28642, while the other groups were considered clinically unacceptable [21]. This finding is supported by another study [13], where post-polymerization times exceeding 60 minutes led to significant differences in color values, with the color of the 3D-printed resins being deemed clinically unacceptable. Considering the levels of perceptibility ($\Delta E00 > 0.8$) and acceptability ($\Delta E00 > 1.8$) commonly used in the literature, all conditions exceed both levels [43]. The porous surface of the printed material, observed in the SEM micrographs, may contribute to color variation, emphasizing the need for surface treatments to improve color stability [44]. Based on the results of this study, a post-polymerization time of 32 minutes is associated with color stability and improved mechanical properties, such as flexural strength.

Regarding translucency, Kim et al. [21] reported less significant changes in printed resins under different hydrothermal aging times after post-polymerization, which is consistent with the results of this study, as the aged groups did not show significant differences among them. They exhibited similarly low levels of translucency after aging, with the initial group without post-polymerization displaying the highest translucency. However, the authors also stated that this variability may depend on the type of printing material used [21].

Within the limitations of this in vitro study, it can be inferred that both the mechanical and optical behavior of the 3D-printed inorganic-filled resin are influenced by its composition, microstructure, manufacturing process, and post-processing, such as post-polymerization. Furthermore, it is clear that hydrothermal aging, simulating intraoral conditions, plays a significant role in this context. However, it is important to highlight that there is an intrinsic variability to each material, which requires more in-depth studies, as the innovation of polymeric materials for 3D printing intended for long-lasting restorations is a growing reality in contemporary dentistry. However, despite advances, this area is still relatively new. Therefore, additional investigations are needed to analyze inorganic-filled polymeric resins used in 3D printing, especially regarding their durability in different conditions, such as on anatomical specimens, as well as their adhesive performance on dental substrates.

CONCLUSION

Within the limitations of this in vitro study, it was concluded that:

- Both the mechanical and optical behavior of the 3D-printed inorganic-filled resin are significantly influenced by factors such as microstructure, chemical composition, post-polymerization times, and hydrothermal aging;
- After hydrothermal aging, there was a reduction in hardness and elastic modulus;
- Flexural strength was significantly influenced by post-polymerization time and hydrothermal aging; although aging affected the flexural strength, the 60- minute aged group exhibited a transient polymer plasticization effect;
- A post-polymerization time of at least 32 minutes was associated with color stability and improved mechanical properties; however, this may affect material translucency.

Acknowledgements

The authors thank the Coordenação de Aperfeiçoamento de Pessoal de Nível Superior – Brasil (CAPES) for the support received.

Data availability

The research data are available in the body of the article.

Author's Contributions

LVCA, NCR: Conceptualization. LVCA, TMBC, JRCSS: Methodology. LVCA, NCR: Writing – Review & Editing. MAB, NCR: Supervision.

Conflict of Interest

No conflicts of interest declared concerning the publication of this article.

Funding

This study was financed in part by the Coordenação de Aperfeiçoamento de Pessoal de Nível Superior – Brasil (CAPES) – Finance Code 001.

Regulatory Statement

Not applicable.

Disclosure

During the preparation of this manuscript, the authors used ChatGPT-5.1 for the purpose of improving readability and linguistic quality during the writing process. After using this tool/service, the authors have reviewed and edited the content appropriately and take full responsibility for the content of the publication.

REFERENCES

1. Andonović V, Vrtanoski G. Growing rapid prototyping as a technology in dental medicine. Mech Eng Sci J. 2010;29(1):31-9.
2. Keating AP, Knox J, Bibb R, Zhurov AI. A comparison of plaster, digital and reconstructed study model accuracy. J Orthod. 2008;35(3):191-201. https://doi.org/10.1179/146531207225022626. PMid:18809782.
3. Liu Q, Leu MC, Schmitt SM. Rapid prototyping in dentistry: technology and application. Int J Adv Manuf Technol. 2006;29(3–4):317-35. https://doi.org/10.1007/s00170-005-2523-2.
4. van Noort R. The future of dental devices is digital. Dent Mater. 2012;28(1):3-12. https://doi.org/10.1016/j.dental.2011.10.014. PMid:22119539.
5. Daher R, Ardu S, di Bella E, Krejci I, Duc O. Ef fi ciency of 3D printed composite resin restorations compared with subtractive materials : evaluation of fatigue behavior, cost, and time of production. J Prosthet Dent. 2024;131(5):943-50. https://doi.org/10.1016/j.prosdent.2022.08.001. PMid:36333176.
6. Flottes Y, Smail Y, Palomino-Durand C, Attal JP, Ceinos R, François P, et al. Properties of 3D printed resins for definitive dental restorations: A systematic review. J Prosthet Dent. 2025;135(4):e6-27. https://doi.org/10.1016/j.prosdent.2025.11.040. PMid:41419355.
7. Abduo J, Lyons K, Bennamoun M. Trends in computer-aided manufacturing in prosthodontics: A review of the available streams. Int J Dent. 2014;2014:783948. https://doi.org/10.1155/2014/783948. PMid:24817888.
8. Tahayeri A, Morgan MC, Fugolin AP, Bompolaki D, Athirasala A, Pfeifer CS, et al. 3D printed versus conventionally cured provisional crown and bridge dental materials. Dent Mater. 2018;34(2):192-200. https://doi.org/10.1016/j.dental.2017.10.003. PMid:29110921.
9. Borella PS, Alvares LAS, Ribeiro MTH, Moura GF, Soares CJ, Zancopé K, et al. Physical and mechanical properties of four 3D-printed resins at two different thick layers: an in vitro comparative study. Dent Mater. 2023;39(8):686-92. https://doi.org/10.1016/j.dental.2023.06.002. PMid:37357046.
10. Mangal U, Seo JY, Yu J, Kwon JS, Choi SH. Incorporating aminated nanodiamonds to improve the mechanical properties of 3d-printed resin-based biomedical appliances. Nanomaterials. 2020;10(5):1-17. https://doi.org/10.3390/nano10050827. PMid:32357463.
11. Aati S, Akram Z, Ngo H, Fawzy AS. Development of 3D printed resin reinforced with modified ZrO2 nanoparticles for long-term provisional dental restorations. Dent Mater. 2021;37(6):e360-74. https://doi.org/10.1016/j.dental.2021.02.010. PMid:33663884.

12. Aati S, Shrestha B, Fawzy A. Cytotoxicity and antimicrobial efficiency of ZrO2 nanoparticles reinforced 3D printed resins. Dent Mater. 2022;38(8):1432-42. https://doi.org/10.1016/j.dental.2022.06.030. PMid:35792014.

13. Kim D, Shim J, Lee D, Shin S, Nam N. Effects of post-curing time on the mechanical and color properties of three-dimensional printed crown and bridge materials. Polymers. 2020;12:2762.

14. Tieh MT, Waddell JN, Choi JJE. Optical and mechanical properties of conventional, milled and 3D-printed denture teeth. J Mech Behav Biomed Mater. 2022;126:105061. https://doi.org/10.1016/j.jmbbm.2021.105061. PMid:34963102.

15. Mchee K, Prause E, Tine DMD, Dmd M, Dmd FB, Dmd JH, et al. Mechanical properties of 3D-printed and milled composite resins for definitive restorations : an in vitro comparison of initial strength and fatigue behavior. J Esthet Restor Dent. 2024;36(2):391-401. https://doi.org/10.1111/jerd.13132. PMid:37680013.

16. Silva GML, Silva SMA, Borba MTLM, Araujo AOS, Torres AJ No, Barreto LAL, et al. Effect of printing angle and aging of a 3D-printed resin for provisional prostheses: an in vitro study on fracture resistance. Braz Dent Sci. 2025;28(2):e4758. https://doi.org/10.4322/bds.2025.e4758.

17. Alp G, Murat S, Yilmaz B. Comparison of flexural strength of different CAD/CAM PMMA-Based Polymers. J Prosthodont. 2018;28(2):e491-5. PMid:29377319.

18. Astudillo-Rubio D, Delgado-Gaete A, Bellot-Arcís C, Montiel-Company JM, Pascual-Moscardó A, Almerich-Silla JM. Mechanical properties of provisional dental materials: A systematic review and meta-analysis. PLoS One. 2018;13(2):e0193162. https://doi.org/10.1371/journal.pone.0193162. PMid:29489883.

19. Keßler A, Hickel R, Ilie N. In vitro investigation of the influence of printing direction on the flexural strength, flexural modulus and fractographic analysis of 3d-printed temporary materials. Dent Mater J. 2021;40(3):641-9. https://doi.org/10.4012/dmj.2020-147. PMid:33456026.

20. Bergamo ETP, Campos TMB, Piza MMT, Gutierrez E, Lopes ACO, Witek L, et al. Temporary materials used in prosthodontics: the effect of composition, fabrication mode, and aging on mechanical properties. J Mech Behav Biomed Mater. 2022;133(June):105333. https://doi.org/10.1016/j.jmbbm.2022.105333. PMid:35839630.

21. Kim JE, Choi WH, Lee D, Shin Y, Park SH, Roh BD, et al. Color and translucency stability of three-dimensional printable dental materials for crown and bridge restorations. Materials (Basel). 2021;14(3):1-15. https://doi.org/10.3390/ma14030650. PMid:33572545.

22. Siqueira JRCS, Rodriguez RMM, Ramos NDC, Bottino MA, Tribst JPM. Immediate and long-term pull-out bond strength of 3D-printed provisional crowns. BioMed Res Int. 2024;2024(1):7205011. https://doi.org/10.1155/2024/7205011. PMid:39263421.

23. Bora PV, Sayed Ahmed A, Alford A, Pitttman K, Thomas V, Lawson NC. Characterization of materials used for 3D printing dental crowns and hybrid prostheses. J Esthet Restor Dent. 2024;36(1):220-30. https://doi.org/10.1111/jerd.13174. PMid:38008797.

24. Espinar C, Della Bona A, Pérez MM, Tejada-casado M, Pulgar R. The influence of printing angle on color and translucency of 3D printed resins for dental restorations. Dent Mater. 2023;39(4):410-7. https://doi.org/10.1016/j.dental.2023.03.011. PMid:36914433.

25. Giacomini MC, Pascon R, Santos MRD, Machado CM, Mosquim V, Jacomine JC, et al. Universal dentin bonding system : influence of handling conditions on the determination of adhesive properties on dentin. Braz Dent Sci. 2025;28(3):1-10. https://doi.org/10.4322/bds.2025.e4782.

26. Bertassoni LE, Marshall GW, De Souza M, Rached N, Universidade P, Paraná C. Effect of pre- and postpolymerization on flexural strength and elastic modulus of impregnated, fiber- reinforced denture base acrylic resins. J Prosthet Dent. 2008;100(6):449-57. https://doi.org/10.1016/S0022-3913(08)60263-2. PMid:19033029.

27. Ramos NC, Luz JN, Valera MC, Melo RM, Saavedra GSFA, Bresciani E. Color stability of resin cements exposed to aging. Oper Dent. 2019;44(6):609-14. https://doi.org/10.2341/18-064-L. PMid:30702414.

28. Adabo GL, dos Santos Cruz CA, Fonseca RG, Vaz LG. The volumetric fraction of inorganic particles and the flexural strength of composites for posterior teeth. J Dent. 2003;31(5):353-9. https://doi.org/10.1016/S0300-5712(03)00049-6. PMid:12799120.

29. Gengenbach TR, Griesser HJ. Deposition conditions influence the postdeposition oxidation of methyl methacrylate plasma polymer films. J Polym Sci A Polym Chem. 1998;36(6):985-1000. https://doi.org/10.1002/(SICI)1099-0518(19980430)36:6<985::AID-POLA14>3.0.CO;2-H.

30. Delgado ANHS, Young AM. Methacrylate peak determination and selection recommendations using ATR-FTIR to investigate polymerisation of dental methacrylate mixtures. PLoS One. 2021;16(6):e0252999. https://doi.org/10.1371/journal.pone.0252999. PMid:34106972.

31. International Organization for Standardization. ISO 10477:2020 - Dentistry-Polymer-Based Crown and Veneering Materials. Geneva: ISO; 2020.

32. Ellakany P, Fouda SM, Mahrous AA, AlGhamdi MA, Aly NM. Influence of CAD/CAM milling and 3D-printing fabrication methods on the mechanical properties of 3-unit interim fixed dental prosthesis after thermo-mechanical aging process. Polymers (Basel). 2022;14(19):4103. https://doi.org/10.3390/polym14194103. PMid:36236050.

33. Sharma G, Wu W, Dalal EN. The CIEDE2000 color-difference formula: implementation notes, supplementary test data, and mathematical observations. Color Res Appl. 2005;30(1):21-30. https://doi.org/10.1002/col.20070.

34. CIE Technical Committee. CIE Technical Report: colorimetry. Vienna, Austria: CIE Central Bureau; 2004. (CIE Pub; no. 15.3).

35. Barszczewska-Rybarek IM, Chrószcz MW, Chladek G. Novel urethane-dimethacrylate monomers and compositions for use as matrices in dental restorative materials. Int J Mol Sci. 2020;21(7):1-23. https://doi.org/10.3390/ijms21072644. PMid:32290163.

36. Leprince JG, Lamblin G, Devaux J, Dewaele M, Mestdagh M, Palin WM, et al. Irradiation modes' impact on radical entrapment in photoactive resins. J Dent Res. 2010;89(12):1494-8. https://doi.org/10.1177/0022034510384624. PMid:20940363.

37. Leprince JG, Palin WM, Hadis MA, Devaux J, Leloup G. Progress in dimethacrylate-based dental composite technology and curing efficiency. Dent Mater. 2013;29(2):139-56. https://doi.org/10.1016/j.dental.2012.11.005. PMid:23199807.

38. Ghavami-Lahiji M, Firouzmanesh M, Bagheri H, Jafarzadeh Kashi TS, Razazpour F, Behroozibakhsh M. The effect of thermocycling on the degree of conversion and mechanical properties of a microhybrid dental resin composite. Restor Dent Endod. 2018;43(2):e26. https://doi.org/10.5395/rde.2018.43.e26. PMid:29765905.

39. Gale MS, Darvell BW. Thermal cycling procedures for laboratory testing of dental restorations. J Dent. 1999;27(2):89-99. https://doi.org/10.1016/S0300-5712(98)00037-2. PMid:10071465.

40. Yao J, Li J, Wang Y, Huang H. Comparison of the flexural strength and marginal accuracy of traditional and CAD/CAM interim materials before and after thermal cycling. J Prosthet Dent. 2014;112(3):649-57. https://doi.org/10.1016/j.prosdent.2014.01.012. PMid:24721504.

41. Buergers R, Rosentritt M, Handel G. Bacterial adhesion of Streptococcus mutans to provisional fixed prosthodontic material. J Prosthet Dent. 2007;98(6):461-9. https://doi.org/10.1016/S0022-3913(07)60146-2. PMid:18061740.

42. Chung SM, Yap AUJ, Chandra SP, Lim CT. Flexural strength of dental composite restoratives: comparison of biaxial and three-point bending test. J Biomed Mater Res B Appl Biomater. 2004;71(2):278-83. https://doi.org/10.1002/jbm.b.30103. PMid:15386492.

43. Paravina RD, Ghinea R, Herrera LJ, Bona AD, Igiel C, Linninger M, et al. Color difference thresholds in dentistry. J Esthet Restor Dent. 2015;27(S1 Suppl 1):S1-9. https://doi.org/10.1111/jerd.12149. PMid:25886208.

44. Yao Q, Morton D, Eckert GJ, Lin WS. The effect of surface treatments on the color stability of CAD-CAM interim fixed dental prostheses. J Prosthet Dent. 2021;126(2):248-53. https://doi.org/10.1016/j.prosdent.2020.05.017. PMid:32829886.

Laura Viviana Calvache Arcila
(Corresponding address)
Universidade Estadual Paulista, Instituto de Ciência e Tecnologia, Departamento de Materiais Odontológicos e Prótese, São José dos Campos, SP, Brazil.
Email: laura.calvache@unesp.br, calvachearcila@gmail.com

Editor-in-chief: Sergio Eduardo de Paiva Gonçalves
Editor: Gabriel Kalil Rocha Pereira

Date submitted: 2025 Oct 30
Accept submission: 2026 May 14